# Universal Drag Force Scaling in High Stokes Number Oscillatory Flows of He II

M. J. Jackson,[1] D. Schmoranzer,[1] L. Doležal,[1] Š. Midlik,[1] T. Skokánková,[1] M. Skyba,[2] J. Bahyl,[3] and L. Skrbek[1]

[1]*Faculty of Mathematics and Physics, Charles University,*
*Ke Karlovu 3, 121 16, Prague 2, Czech Republic.*
[2]*Institute of Physics ASCR, v.v.i., Na Slovance 2, 182 21, Prague 8, Czech Republic.*
[3]*Faculty of Mathematics, Physics and Informatics,*
*Comenius University, Mlynská dolina F1, Bratislava, Slovak Republic.*

We present a unified analysis of the drag forces acting on oscillating bodies submerged in superfluid $^4$He - He II: vibrating wire resonator, tuning fork, double-paddle, and torsionally oscillating disc. We find that in the two-fluid temperature range above 1 K, for high Stokes number oscillatory flows (viscous penetration depth in the normal fluid much smaller than the characteristic size of the oscillator), the drag forces originating from the normal component of He II are described in terms of suitable dimensionless parameters and exhibit a clearly defined universal scaling behavior, derived by modification of classical fluid dynamical laws and verified in classical fluids. We use this approach to illustrate the transition from laminar to turbulent drag regime in He II oscillatory flows and compare the critical velocities associated to the production of quantized vorticity in the superfluid component with the critical velocities for the first flow instabilities occurring in the normal component. We show that, depending on the temperature and geometry of the flow, either type of instability may occur first – we even demonstrate a crossover caused by temperature dependence of the kinematic viscosity of the normal fluid – and over certain range of parameters may exist on its own, but eventually acts as a trigger for the other one. At temperatures below 1 K, a transition to a ballistic regime occurs in He II and we develop a formalism allowing direct comparison between measurements with resonators in He II and (nanomechanical) oscillators in classical dilute gases.

March 2, 2018

## I. PREFACE

Historically, experiments on oscillatory flows of classical viscous fluids have been studied since the days of G. G. Stokes [1], with many notable developments made in the last century mainly dealing with oscillating cylinders [2–5]. In the modern era, oscillating flows have gained notoriety thanks to developments in micro- and nanomechanical engineering, where access to MEMS/NEMS devices has offered unprecedented sensitivity and resolution in fluid dynamical experiments, allowing the transition from continuum to the ballistic (kinetic) regime to be probed at easily attainable pressures, formulate universality relations [6–8] and directly probe fluid boundary layers [9].

An extremely broad range of working fluids may be obtained when traversing the different phases of helium, even limiting ourselves to the common isotope $^4$He. The normal liquid phase of $^4$He - He I and cryogenic He gas are very interesting working fluids thanks to their extremely low kinematic viscosity, $\nu$ [10], which provide very high Reynolds number (Re $\approx 10^7$) flows in controlled laboratory experiments [11, 12] or extremely large Rayleigh numbers (Ra $\approx 10^{17}$) in buoyancy driven flows such as Rayleigh-Bénard convection [13], thanks to the very high value of the combination of physical properties $\alpha_{\rm th}/(\nu\kappa_{\rm th})$, where $\alpha_{\rm th}$ is the thermal expansion and $\kappa_{\rm th}$ stands for the thermal diffusivity [14, 15]. Normal liquid $^4$He, known as He I, at $T_\lambda \approx 2.17$ K undergoes a second-order superfluid transition. Superfluid $^4$He – He II – is a quantum fluid, and its flow properties cannot be described by the Navier-Stokes equation. According to the two-fluid model [16, 17], it behaves as if composed of two inter-penetrating liquids - the normal and superfluid components - with corresponding velocity fields and temperature-dependent densities. While the normal fluid behaves classically, possessing finite viscosity and carrying the entire entropy content of He II, the superfluid component has neither entropy nor viscosity and, due to quantum restrictions, the vorticity is constrained into line singularities called quantized vortices. Quantum turbulence [18] (in He II above about 1 K, where appreciable amount of normal fluid exists) therefore takes the form of a tangle of quantized vortices in the superfluid component which typically coexist with classical-like turbulent flow of the normal fluid. In the presence of quantized vortices, the otherwise independent normal and superfluid velocity fields become coupled by the mutual friction force which arises due to quasiparticles scattering off the cores of quantized vortices.

Oscillatory quantum flows of He II have been studied using various oscillators such as discs [19, 20], piles of discs [21], spheres [22–24], grids [25–27], tuning forks [28–31], reeds [32], cylinders of rectangular [33] or circular cross-section (wires) [34–37] since the discovery of superfluidity, and have lead to important insights to this fundamental physical phenomenon. For reviews, see [38, 39]. Nevertheless, a universal picture of scaling in superfluid hydrodynamics is still missing, which motivated us to investigate a special class of oscillatory quantum flows of He II due to mechanical oscillators of different geometries

– a vibrating tuning fork, a microwire loop, a torsionally oscillating disc and a double paddle [40–42]. We find that for high Stokes number oscillatory flows (viscous penetration depth in the normal fluid much smaller than the characteristic size of the oscillator), the drag forces originating from the normal component of He II are described in terms of suitable dimensionless parameters and exhibit a clearly defined universal scaling behavior. We identify and compare the critical velocities related to the production of quantized vorticity in the superfluid component with the critical conditions for the instabilities occurring in the normal component. We find that either type of instability may occur first and over certain range of parameters exist on its own. We even demonstrate a crossover between these first instabilities, caused by temperature dependence of the kinematic viscosity of the normal fluid. Either instability eventually acts as a trigger for the other one, depending on the temperature and geometry of the flow.

Additionally, for temperatures below 1 K where a transition to a ballistic regime occurs in He II, a formalism is developed based on the theory of ideal Bose gases allowing direct comparison between experiments performed in the ballistic regime of the superfluid and in dilute classical gases. Consequently, standard cryogenic techniques such as dilution refrigeration [43] provide as a testing ground for MEMS/NEMS devices, extending the available range of the ballistic regime in He II by simply changing its temperature.

## II.   INTRODUCTION

### A.   Superfluid Hydrodynamics

On a phenomenological level, superfluid $^4$He - He II is at finite temperatures described as consisting of two components - a viscous normal component and an inviscid superfluid component. Their temperature-dependent densities, $\rho_N$ and $\rho_S$ make the (nearly temperature independent) total density of He II, $\rho$. With no quantized vortices present, isothermal flows of both components have independent velocity fields, and both can easily become turbulent.

Does quantum turbulence always contain quantized vortices? Strictly speaking, if one takes the definition of quantum turbulence as turbulence occurring in quantum fluids displaying superfluidity and the two-fluid behavior literary, quantized vortices are not the necessary ingredient of quantum turbulence. One can imagine a two-fluid flow of He II consisting of turbulent normal flow and potential superflow. Indeed, in the hypothetical case of a macroscopic sample of He II free of quantized vortices (i.e., without mutual friction aiming to couple the two velocity fields), in an isothermal flow the normal and superfluid components move independently and instability criteria ought to be applied to them separately. In this hypothetical case quantized vortices must be nucle-

ated intrinsically; this process requires critical velocities of order 10 m/s or higher. In practice, however, remnant vortices always exist in macroscopic samples of He II and nucleation of quantized vorticity takes place extrinsically, by stretching and reconnections of seed vortex loops. In many types of flow the critical velocity for extrinsic vortex nucleation is observed to be a few cm/s. It follows that there indeed is a possibility of having a quantum flow displaying (nearly) potential superflow superimposed on vortical flow of the normal component.

At the macroscopic level, the dynamics of mechanically forced He II flow (i.e., flows with no forcing difference between the mean superfluid and normal fluid flows, called coflows) may be described in a continuous fashion by the coarse-grained HVBK equations [17, 44] based on Landau's two-fluid model [16]. This description allows for the coexistence of turbulence in the superfluid component and classical turbulence in the normal component, but is valid only for temperatures above about 1 K. Further simplification is possible, if the superfluid and normal components do not interact significantly, which physically requires negligible vortex line density in the superfluid component. Then the HVBK equations simplify so that the motion of the normal component is described by a Navier-Stokes type equation, while that of the superfluid component by the Euler equation for ideal fluids. Under these conditions, any body moving through He II at low velocity below the (generally independent) thresholds, would experience drag forces originating from the normal component alone, while the drag forces offered by the superfluid component are zero (neglecting any drag due to surface waves and compressibility effects). In this case the superfluid component can be understood as a physical vacuum, merely re-normalizing the effective mass of the oscillating body. Therefore, to derive the scaling laws for the drag forces, we start our analysis from the Navier-Stokes type equation governing the motion of the normal component.

### B.   Oscillatory Viscous Flows

To describe oscillatory hydrodynamic flow, the governing Navier-Stokes equations may be expressed in terms of a dimensionless velocity $\boldsymbol{u'} = \boldsymbol{u}/U$, time $t' = t/T$ and positions $\boldsymbol{r'} = \boldsymbol{r}/L_i$ as:

$$\frac{U}{T}\frac{\partial \boldsymbol{u'}}{\partial t'} + \frac{U^2}{L_1}(\boldsymbol{u'} \cdot \boldsymbol{\nabla'}\boldsymbol{u'} + \boldsymbol{\nabla'}p') = \frac{\nu_N U}{L_2{}^2}\Delta'\boldsymbol{u'}, \qquad (1)$$

where the characteristic length scales $L_{1,2}$ are used together with the characteristic velocity $U$ to estimate the maximum magnitude of the respective velocity derivatives. An independent time scale $T$ is introduced, given by the period of oscillation. Generally, the choice of $L_1$ and $L_2$ depends on body geometry and flow parameters. Candidates may include the typical body size $D$, the surface roughness, or the Stokes boundary layer thickness (viscous penetration depth), which may be defined as

$\delta = \sqrt{2\eta/(\rho\omega)}$, where $\omega$ is the angular frequency of oscillations and $\eta$ denotes the dynamic viscosity of the working fluid. If, for a given body $\delta \ll D$, one may say that the body oscillates in the high-frequency regime, which is equivalent to the high Stokes number $\beta = D^2/(\pi\delta^2) \gg 1$.

In the high frequency limit, depending on body geometry (especially surface roughness and the presence of sharp corners), $\delta$ or $D$ may take the part of $L_1$ (related to the largest tangential velocity derivative) in the Navier-Stokes equation, but it is always $\delta$ that takes the part of $L_2$ (related to the largest velocity derivative in any direction). When the surface roughness exceeds $\delta$, we may put $L_1 = L_2 = \delta$, and the Navier-Stokes equation may be written using only one dimensionless parameter, the boundary layer-based Reynolds number: $Re_\delta \equiv (\delta\rho U)/\eta$. Conversely, for a hydrodynamically smooth body ($\delta$ exceeds the surface roughness) without sharp corners such as a cylinder, we would obtain the Navier-Stokes equation with the Keulegan-Carpenter number $K_C = UT/D$ as the only relevant dimensionless parameter, as expected [2].

## C.  Oscillatory Flows of He II

Assuming two independent velocity fields in He II, the above considerations are fully applicable for the oscillatory viscous flow of the normal component. We therefore have to replace $\delta$ by $\delta_N = \sqrt{2\eta/(\rho_N\omega)}$, where $\eta$ denotes the dynamic viscosity of He II. Again, if, for a given body $\delta_N \ll D$, one may say that the body oscillates in the high-frequency regime, which is equivalent to the high Stokes number regime $\beta_N = D^2/(\pi\delta_N^2) \gg 1$ and in the Navier-Stokes equation $\delta_N$ always takes the part of $L_2$ (related to the largest velocity derivative in any direction). When the surface roughness exceeds $\delta_N$ (typically or order 1 $\mu$m in our experiments), we may put $L_1 = L_2 = \delta_N$, and the Navier-Stokes equation may be written using only one dimensionless parameter: $Dn \equiv (\delta_N\rho_N U)/\eta$, which we call the Donnelly number [45].

If $\delta_N \ll D$ is satisfied, and no turbulence (neither in the superfluid nor the normal component) is produced, the flow of the superfluid component will be potential and the normal component will exhibit laminar viscous flow inside the boundary layer, remaining approximately potential outside. In that case, the magnitude of the viscous drag force may be estimated as:

$$F = \eta \oint \frac{du_i}{dn_j}dS_j \approx \eta S_{\text{eff}}U/\delta_N = US_{\text{eff}}\sqrt{\eta\rho_N\omega}, \quad (2)$$

where an effective surface area $S_{\text{eff}} \geq S$ may be used to account approximately for the surface roughness. The dimensionless drag coefficient related to the normal component becomes:

$$C_{DN} = \frac{2F}{A\rho U^2} = \frac{2S_{\text{eff}}}{A}\frac{\sqrt{\eta\rho_N\omega}}{\rho U} \quad (3)$$

and may be expressed in terms of the Donnelly number as $C_{DN} = \alpha/Dn$, where $\alpha = 2S_{\text{eff}}/A$. Thus in the laminar case, the normal component is fully described by classical laws.

To facilitate the hydrodynamic description of the superfluid component, we define the superfluid drag coefficient

$$C_{DS} = \frac{2F}{A\rho_S U^2} . \quad (4)$$

The instability leading to the production of quantized vorticity is related to self-reconnection of seed vortex loops and has been sufficiently discussed in the literature [22, 46]. The related critical velocity $U_C$ is expected to scale as $U_C \propto \sqrt{\kappa\omega}$, where $\kappa = 0.997 \times 10^{-7}$ m$^2$s$^{-1}$ is the quantum of circulation in He II. Hence, it is convenient to define a reduced dimensionless velocity $\hat{U} = U/\sqrt{\kappa\omega}$.

In the turbulent drag regime, at velocities sufficiently above the critical values, the normal and superfluid components of He II are expected to be coupled due to the mutual friction force and contribute to the pressure drag. In this situation, the classical definition of the drag coefficient may be used: $C_D = 2F/(A\rho U^2)$, where the total density of He II $\rho = \rho_N + \rho_S$ is used. It is expected that in coupled turbulent flows, this drag coefficient will tend towards a temperature-independent constant value [38, 47].

Note in passing that the described approach is only approximate, as it neglects the streaming flow that is known to exist in the vicinity of the oscillating objects and in highly turbulent flow due to vibrating quartz turning fork has been recently even visualized in He II [33]. For relatively slow velocities in our experiments in this study the contribution of this streaming flow to the drag can be in most cases safely neglected.

## D.  Ballistic Regime

In classical fluids, when the molecular mean free path $\lambda$ becomes comparable to a characteristic dimension of the system $D$, or the frequency of the flow $\omega$ becomes comparable to the inverse relaxation time $\tau$ of the fluid towards equilibrium, the continuum hypothesis starts to break down and the Navier-Stokes equations no longer represent a valid description of the system. On a fundamental level, such systems ought to be described by a particle distribution function, evolving according to the Boltzmann kinetic equation. In the transitional regime, where $\lambda \simeq D$ (or $\omega\tau \simeq 1$), extensions of the continuum approach are often employed, and quantities of interest are typically calculated as series expansions in terms of the Knudsen number $Kn = \lambda/D$, or the Weissenberg number $Wi = \omega\tau$. This typically happens in gases at low pressures of order 1 Pa, or in viscoelastic media.

In superfluid helium, a similar situation occurs as the temperature is reduced below 1 K. Since the excitation

density decreases very rapidly with decreasing temperature, the mean free path of thermal excitations making up the N component becomes comparable with the dimensions of the experiment around 0.7 K. Below 0.7 K, He II is better described as a gas of thermal quasiparticles propagating ballistically through a physical vacuum of the superfluid component [48, 49], which only enhances the effective masses of accelerating objects, but exerts no drag force unless QT is produced.

Despite the notable differences in the underlying physics, a formalism may be developed relating the gas of thermal excitations to classical dilute gases, leading to a definition of quasiparticle pressures and estimates of their mean free paths. This formalism may be used to directly compare measurements in superfluid helium to the results obtained in dilute classical gases using MEMS/NEMS structures [6–8], which indicate that a universal description of oscillatory flows may be possible. Verifying the proposed universality relations in a gas of quasiparticle excitations would yield very strong evidence in their support, especially considering that the range of experimentally attainable pressures may be extended by several orders of magnitude in superfluid helium. The details relating to the thermal excitations and the proposed formalism are given in Section Discussion.

### E. Additional Dissipation Mechanisms

In our recent work [31] we investigated the behavior of oscillatory flow due to quartz tuning fork in isotopically pure superfluid He II in the zero temperature limit. We have shown that the linear damping forces can be fully described and understood as a combination of tuning fork intrinsic damping (dominant at lowest temperatures) and ballistic phonon drag $\propto T^4$, which gradually changes into hydrodynamic viscous damping at higher temperatures, relevant to this study. It was only at the lowest temperatures, where the role of the steeply frequency dependent intrinsic damping due to stress-strain hysteresis in the quartz was apparent – it can be safely neglected in this study. Additionally, even comparatively larger losses due to sound emission through the surrounding fluid can be safely neglected for the fundamental mode of the tuning fork and represents perhaps a very small contribution to the overtone damping [50]. Based on our previous study of acoustic emission by oscillating objects in He II, this statement holds for all oscillators used in this work [51].

### F. Multiple Critical Velocities

A number of experimental studies reported observation of more than one critical velocity of hydrodynamic origin. At milliKelvin temperatures, they have been observed in oscillatory flows of He II due to vibrating wires [36], grids [25, 26] or tuning forks [29, 52]. Recently we have presented convincing evidence for even three distinct hydrodynamic critical velocities and proposed explanation linking all the observations of oscillatory flow in zero temperature limit into a single framework. [31]. In short, the first critical velocity, connected mostly to frequency shifts rather than changes in the drag force, is associated with the formation of a number of quantized vortex loops near the surface of the oscillator, possibly forming a thin layer, which affects the coupling to the fluid and thus the hydrodynamic added mass. This first critical velocity is hardly observable in the two-fluid regime. The second critical velocity is related to the quantized vorticity propagating into the bulk of the superfluid, either in the form of emitted vortex loops or, eventually, as a turbulent tangle. It is always accompanied by a marked increase in the drag force and usually hysteresis (detectable with amplitude sweeps). It is this critical velocity which we are dealing with in this work. For completeness, there is the third and highest critical velocity of hydrodynamic origin, above which the drag coefficient starts to grow towards unity. We proposed that it is linked to a qualitative change in the pattern of quantized vorticity, during which the vortex tangle becomes partly polarized, developing larger structures, and on scales exceeding the quantum length scale starts to mimic classical turbulence generated by oscillating objects in viscous fluids. As the third critical velocity was found very high, of order m/s, it is unlikely that it was reached in the reported here experiments.

## III. EXPERIMENTAL DETAILS

The resonators used in our investigation - the wire, the tuning fork, the torsionally oscillating disc and the double paddle - were driven (except the disc) and monitored by the developed by us LabView software. The driving voltage/current was provided by an Agilent A33220 signal generator, and a phase-sensitive Stanford Research SR830 lock-in amplifier measured both the in-phase and out-of-phase components of the induced signals.

Most of the measurements were performed in a helium immersion cryostat during a dedicated experimental run for each resonator. The helium bath is brought down to the desired temperature using a rotary pump and a Roots pump and stabilized on the level of few mK either manually, by adjusting the pumping speed, or using a temperature controller. The lowest attainable temperature - $1.265\,\mathrm{K}$ - allows access to most of the two-fluid regime.

### A. Vibrating Wire Resonator

Vibrating wire resonators are well-established low temperature probes [53]. They consist of a semi-circular loop of wire subjected to a vertical magnetic field $B$, as shown in Fig. 1. A loop is used to prevent closely spaced or degenerate resonate modes one may observe on a straight
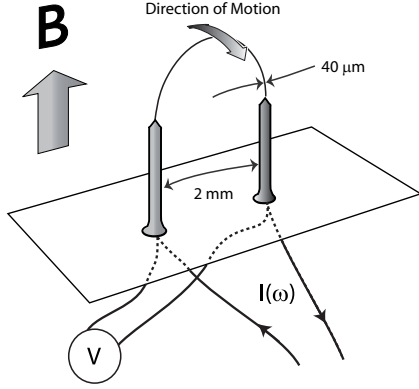
wire.



FIG. 1. Schematic diagram of a vibrating wire resonator.

Passing an alternating current $I(\omega)$ through the wire forces it to oscillate due to the Lorentz force, $F_L = BDI$. As the wire moves through the magnetic field, it induces a voltage which can be determined using Faraday's law. For a rigid semi-circular wire with leg spacing $D$, oscillating at a peak velocity $U$, the area bounded by the loop $A = \pi D^2/8$ and the rate of change of angle to the field is $2U/D$. Therefore, the induced Faraday voltage generated by a semi-circular vibrating wire loop is given by:

$$V = -\frac{d(\boldsymbol{B} \cdot \boldsymbol{A})}{dt} \simeq \frac{\pi}{4} BDU. \tag{5}$$

The vibrating wire resonator used in this study consists of a semi-circular loop $40\,\mu$m superconducting NbTi wire with a leg spacing of 2 mm. The wire was mounted in a brass cell submerged in the bulk superfluid and mounted between a pair of permanent magnets in a magnetic field of $170 \pm 10\,$mT at room temperature. We estimate that the field is reduced by approximately 20% at low temperatures [54].

### B. Quartz Tuning Fork

Quartz tuning forks are piezoelectric oscillators with a calibrated resonant frequency, often used as frequency standards or shear force sensors for scanning optical microscopes [55]. Quartz tuning forks are now well-established probes of cryogenic helium flow [28]. The fork used in this study is of the following dimensions: length of the prongs $L_{\mathrm{f}} = 3.50\,$mm, tine thickness (parallel to the direction of motion) $T_{\mathrm{f}} = 90\,\mu$m and width $W_{\mathrm{f}}$ = $75\,\mu$m (original wafer thickness). Its two prongs are separated by $D_{\mathrm{f}} = 90\,\mu$m. A sketch of the fork including these dimensions is shown in Fig. 2. There are two different readily accessible flexural resonant modes – the fundamental resonance at 6.5 kHz and the first flexural overtone at 40.0 kHz.
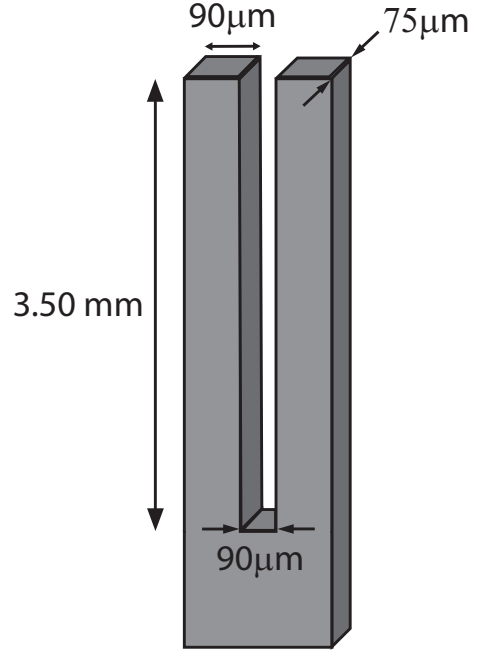


FIG. 2. Schematic diagram of the quartz tuning fork.

The fork is driven by applying an ac voltage $V$ from a function generator to the metallic electrodes deposited on the surface of the quartz. This produces a force proportional to the voltage which sets the two prongs oscillating in anti-phase along the direction $T_{\mathrm{f}}$. The distortion of the quartz induces a piezoelectric-current $I$ which is proportional to velocity $U$. The relations between force, velocity, voltage and current are:

$$F = \frac{a_{rmf}V}{2}; \quad I = a_{rmf}U \tag{6}$$

where $a_{rmf}$ is the so-called fork constant, which may be obtained through calibration by deflection measurement or self-calibration in vacuum, in which case it is given as $a_{rmf} = \sqrt{4\pi m_{\mathrm{f}}^{\mathrm{eff}} \Delta f I/V}$, where $m_{\mathrm{f}}^{\mathrm{eff}}$ is the effective mass of the fork, and $\Delta f$ is the measured half-height resonant width [28]. The effective mass [50] of the tuning fork is given by $m_{\mathrm{f}}^{\mathrm{eff}} = T_{\mathrm{f}}W_{\mathrm{f}}L_{\mathrm{f}}\rho_{\mathrm{q}}/4$, where $\rho_{\mathrm{q}} = 2650\,\mathrm{kg\,m}^{-3}$ is the density of the fork material (quartz). The ac current is measured using an IV-converter [56] and a SR-830 lock-in amplifier. The standard measurement scheme used here can be found, e.g., in Fig. 1 of Ref. 31.

### C. Double Paddle

Recent studies [41, 42] have shown that the so called double-paddle resonators may serve as promising probes to study superfluid hydrodynamics. These have demonstrated high quality factors, compared to other mechanical resonators since any vibrational losses are heavily suppressed through their base.
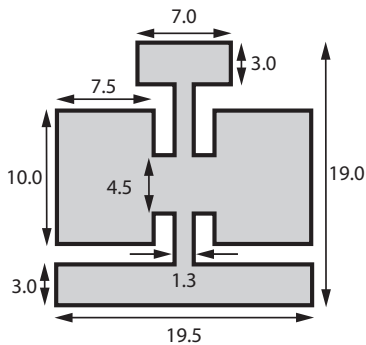
FIG. 3. Schematic diagram of the double paddle oscillator. The dimensions are in millimetres. The $\langle 110 \rangle$ silicon wafer has a thickness of 0.25 mm.



FIG. 4. Schematic diagram of the torsionally oscillating disc.

Here, we employ the same silicon double paddle oscillator etched from a 0.25 mm thick $\langle 110 \rangle$ silicon wafer, as previously used by Zemma and Luzuriaga [41], sketched in Fig. 3. The two larger side paddles are approximately 10 mm × 7.5 mm and the smaller upper paddle is 7 mm × 3 mm. The paddle is driven magnetically, by attaching a small magnet located between the paddles in the oscillator stem; its displacement is detected capacitively. In order to generate the oscillatory motion, an ac current is applied to a small superconducting coil fixed to the support frame.

### D. Torsionally Oscillating Disc

The torsional oscillator consists of a 0.05 mm tungsten wire 32 cm long with a borosilicate glass disc fixed to the wire at its midpoint using a thin 0.8 mm brass capillary and Stycast 2850. The disc is 1 mm thick with a diameter of 40 mm (a schematic diagram is shown in Fig. 4). When the wire is under tension, the disc is positioned approximately midway between the two polished FR2 plates 10 mm apart (both disc sides were approximately 4.5 mm away from the FR2 plate facing them). Sixteen black marks around the circumference of the disc are used to determine the deflection and angular velocity of the disc from the recorded sequences.

The motion of the disc is recorded with a Canon EOS 600D digital camera fitted with a Canon EF-S 18-135 mm f / 1:3.5 - 5.6 IS lens. The recordings presented here were acquired at the frame rate of 240 fps with a resolution of 512×384 pixels.

Our raw data is in the form of video recordings of the motion of the disc during the experiments. Because the marks on the disc are relatively small compared to the entire field of view, with rather low contrast to the not-entirely-uniform background, standard motion tracking software could not be used to process the videos. Hence, fairly complex post-processing is required to extract quantitative and interpretable data.

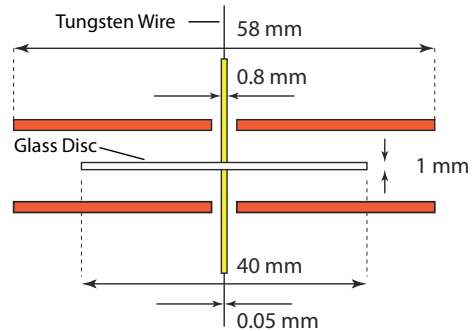The video is split into individual frames, de-interlacing them in the process, which means that only pixels recorded at exactly the same time are kept. The color images are converted to monochromatic bitmaps so the marks appear as black spots on a white background. These monochromatic bitmaps are then analyzed by a custom-made program which localizes the black areas in each image and evaluates their size and center-of-mass. It then assignes individual dots between consecutive images to each other (making special arrangements for those not reproduced in some of the bitmaps) and calculates the average displacement between the two frames in pixels (see Fig. 5). This basically gives us a value of the circumference's velocity in pixels per frame. This velocity is then converted into an angular velocity, assuming that the optical effects due to several curved glass plates are negligible as only the central region of the field of view is kept for processing.
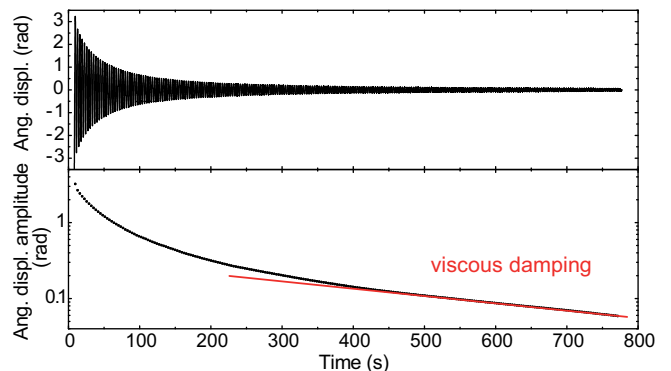


FIG. 5. Typical measurement of angular displacement of the torsionally oscillating disc as a function of time. (Top) The signal extrema were evaluated to obtain the angular displacement amplitude, $\phi_0$. The logarithmic plot (Bottom) clearly shows two distinct regions – exponential (viscous) decay due to laminar flow of the normal component for $t \gtrsim 500$ s and a faster decay at earlier times.

## IV.   EXPERIMENTAL RESULTS AND ANALYSIS

In this section we present our drag force measurements by using the resonators introduced above. We then isolate the sources of the various drag forces acting on the structures, in particular, by separating the contributions due to the two fluid components.

In our previous study of tuning forks in He II at very low temperatures [31], it was shown how important it is to perform full frequency sweeps across the resonant response of the oscillators. These full sweeps, at fixed drive level, reveal important details relevant to the onset and the nature of any nonlinear behavior, displaying complex features in the resonant response such as various hysteretic phenomena. On the other hand, simple and less time consuming amplitude sweeps at fixed resonant frequency might uncover hysteretic features that might otherwise have been overlooked by amplitude sweeps, and we therefore paid attention to check the resonant response in both ways.

### A.   Vibrating Wire Resonator

The resonant response of the vibrating wire resonantor is obtained by measuring the voltage in phase with the driving current, as a function of frequency. In Fig. 6, we plot the resonant frequency response of the vibrating wire at various drives at 1.67 K. The velocity of the top part of the wire is known with the accuracy about ±20%, as the actual value of the magnetic field produced by the pair of permanent magnets has not been calibrated at low temperature. Assuming that at investigated low temperatures the magnetic field is constant and that the velocity is proportional to it, this does not affect the scaling of the drag discussed later. For small drive levels, the frequency response is of Lorentzian form. Upon increasing the drive level, the Lorentzian shape becomes distorted and the resonant frequency shifts towards lower frequencies. The flattening of the peak indicates the onset of non-linear drag forces typically associated with instabilities in the generated oscillatory flow.

In Fig. 7, we plot the peak velocity $U$ as a function of driving force $F$ at various temperatures. Each point represents the results of a pair of full frequency sweeps; one measured with increasing, the other with decreasing frequency, which allows us to identify any hysteretic behavior.

At low velocities, the wire exhibits linear damping at all temperatures. The loses from the wire in this region are due to intrinsic mechanical loses, acoustic emission and dominated by temperature-dependent hydrodynamic viscous drag due to the normal fluid component.

Upon reaching some critical velocity, the response changes, indicating an extra dissipation mechanism which eventually begins to dominate. The damping force gradually becomes proportional to $U^2$ and independent
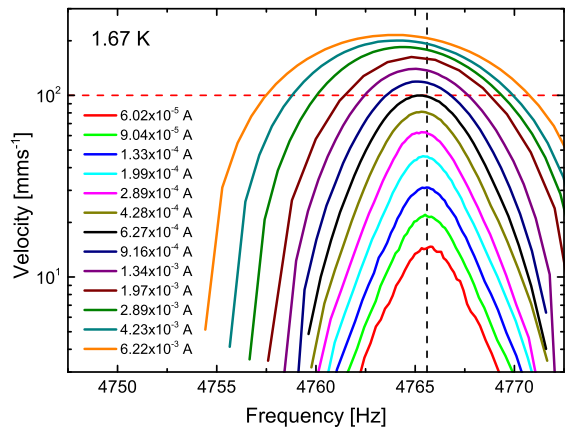


FIG. 6. Resonant frequency response of the vibrating wire resonator at various drives at a temperature of 1.67 K. The black vertical dashed line marks the position of the resonance peak at low drives. The red dashed line highlights the estimated velocity at which the frequency-softening sets in and the frequency shift becomes apparent.
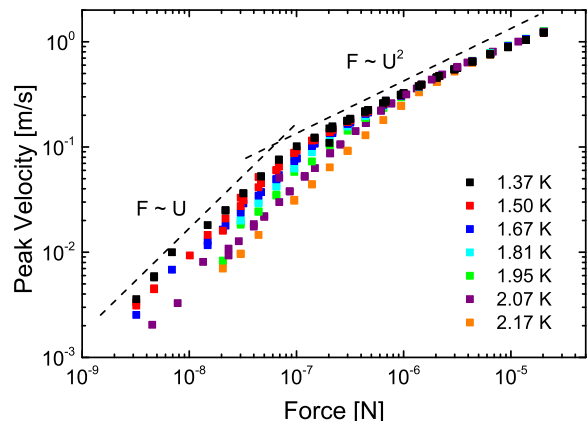


FIG. 7. Peak velocity as a function of the peak driving force applied to the vibrating wire submerged in superfluid $^4$He at temperatures as indicated. The dashed lines serve as guides to the eye.

of temperature $T$, in the studied temperature range, $1.293\,\mathrm{K} \leq T \leq 2.170\,\mathrm{K}$. We note that in classical viscous fluid the damping force in the turbulent drag regime is proportional to $U^2$ [57].

The drag coefficient as a function of velocity for the vibrating wire are plotted in Fig. 8; the drag coefficient being evaluated using the data presented in Fig. 7. To calculate the drag coefficient $C_D = 2F/(A/\rho U^2)$ from the dissipative force $F$ (which is equal to the driving force), we use the peak wire velocity $U$ and we assume that $A$ is the projected cross-section of the wire in perpendicular to the wire's direction of motion. Here the relevant fluid density is the total density of $^4$He at any given temperature.
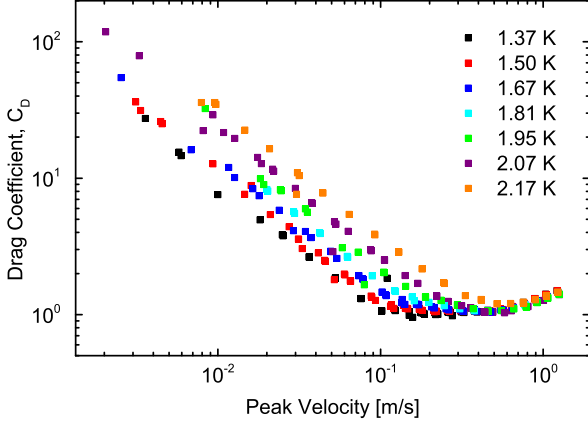
FIG. 8. Drag coefficient as a function of peak velocity for the vibrating wire at various temperatures as indicated.

In order to isolate the contribution of the normal fluid component to the drag forces acting on the wire, we redefine the drag coefficient using the normal fluid density and we plot it as a function of the Donnelly number (see Fig. 9).
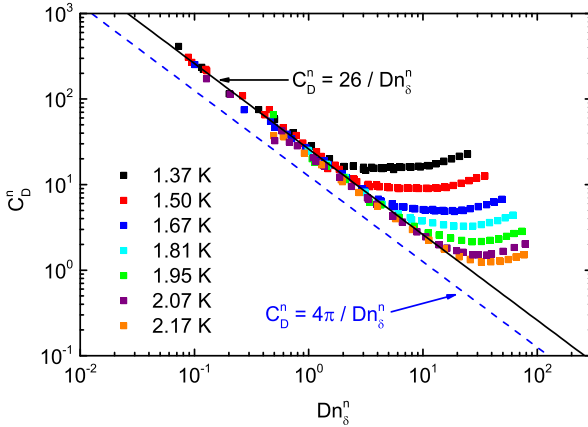


FIG. 9. Normal fluid's contribution to the drag coefficient as a function of the Donnelly number for the vibrating wire at various temperatures as indicated. The blue dashed line shows the expected dependence for a smooth cylinder. The solid black line is an empirical fit to the linear data.

Universal scaling is observed for the wire, however, we note that the pre-factor for the laminar scaling is somewhat larger than one would expect for a smooth cylinder. This is most likely due to the surface roughness and excrescences left on the wire during the ablation of the wire's insulation and variations in the cross section of the wire caused by extrusion during the manufacturing process, effectively increasing the surface area of the wire and extending the viscous penetration depth.

## B. Tuning Fork

The resonant response of the quartz tuning fork is again obtained by measuring the current in-phase with the driving voltage as a function of frequency. The electrical quantities are then converted into mechanical quantities, as explained in the previous Section. By performing frequency sweeps in vacuum at low temperature, the experimental fork constant is estimated to be $a_f = 3.665 \times 10^{-7}$ C/m and $a_f^o = 1.409 \times 10^{-6}$ C/m for the fundamental mode and overtone, respectively.

On resonance, the driving force is in equilibrium with the dissipative drag force acting on the prongs. The power dissipated by the fork is assumed to be equal to the supplied electrical power given by $\dot{Q} = FU = IV/2$. We estimate that the fork constant has an uncertainty of 10% since it was shown that the optically-measured prong velocity is actually 10% lower [58] than that determined from the electro-mechanical model described in section III B.
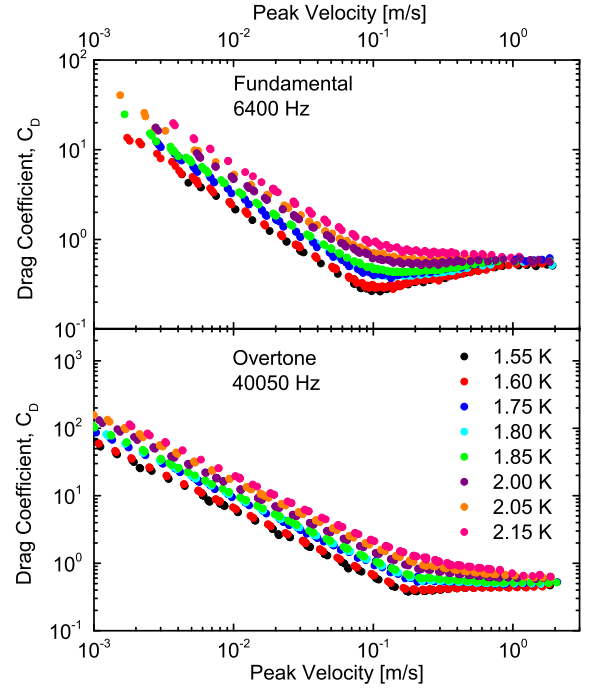


FIG. 10. Dimensionless drag coefficient as a function of peak velocity for the fundamental mode (Top) and overtone (Bottom) of the tuning fork at various temperatures.

In Fig. 10, we plot the drag coefficient as a function of the peak velocity for the fundamental mode of the fork at various temperatures. To calculate the drag coefficient from the dissipative force $F$, we have assumed that $A$ equals to the cross-sectional area of a tuning fork prong perpendicular to its motion, $W_f L_f$, that the relevant fluid density is the total density of He II, and we use the tuning fork peak velocity for $U$.

As expected, the tuning fork exhibits linear damping at low velocities at all temperatures. Upon increasing

the velocity, changes in the drag coefficient's velocity dependence can be observed occurring at approximately $10^{-1}$ m/s and are independent of temperature in the assessed temperature range.

At high velocities, the drag coefficient tends to a temperature dependent constant value of order unity ($C_D \approx 0.6$) as one would expect for a classical viscous fluid. One might anticipate that, at very high velocities, the drag will not depend on whether the fluid is superfluid or not. In our case, there is little change in the drag coefficient at high velocities over the full temperature range and we therefore conclude that the two fluids must be coupled in the fork's vicinity by mutual friction and the flow due to the fork behaves as a classical-like fluid in the turbulent drag regime.

On decreasing temperature, the drag coefficient falls over the whole range of velocities as the fraction of the normal fluid component decreases. This indicates that the drag is largely dominated by the normal fluid component.

To characterize the normal fluid component's flow, we plot the normal fluid's contribution to the drag coefficient as a function of the Donnelly number for both of the tuning fork's modes in Fig. 11. At low Donnelly numbers, the data collapse to a single dependence before deviating at some critical value. This critical Donnelly number pinpoints the location of the instability in the flow and an onset of crossover from laminar to turbulent drag regime.
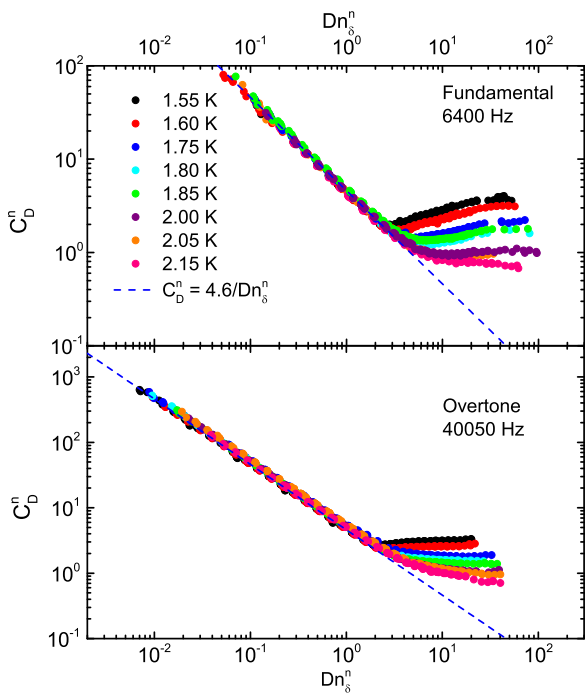


FIG. 11. Normal fluid drag coefficient as a function of the Donnelly number for the fundamental mode (Top) and the overtone (Bottom) of the tuning fork at the various indicated temperatures.

It is interesting to note that despite the difference in

the velocity profile and the viscous penetration depth, the same pre-factor for the laminar scaling is displayed for the two modes of oscillation.
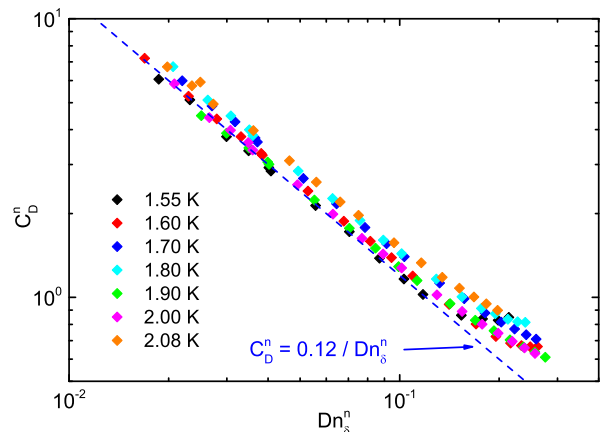


FIG. 12. Normal fluid drag coefficient as a function of the Donnelly number calculated for the silicon double-paddle of Zemma and Luzuriaga[41].

## C. Double Paddle

We now apply the same analysis to results obtained using a silicon double paddle oscillator by Zemma and Luzuriaga [41]. We analyze the symmetric torsion mode [40] data. In vacuum at $4.2$ K, the resonant frequency of the paddle is $520$ Hz, in liquid helium at $4.2$ K it is was $358$ Hz. The viscous penetration depth is $\approx 3\,\mu$m. Since the characteristic length scale of the paddle is $D \approx 1$ cm, the paddle is operating in the high Stokes number limit, which means our analysis is justifiable.

In Fig. 12, we present the normal fluid drag coefficient plotted against the Donnelly number. The viscous drag force collapses to a single dependence demonstrating that the paddle is indeed in the high-frequency limit, backing up our claim that scaling due to the drag force offered by the normal fluid is universal.

Closer inspection of the data shows, however, that the source of the initial instabilities is not entirely clear. To address this, we plot the normalized non-linear drag force as a function of the Donnelly number for the double paddle in Fig. 13. At high temperatures (for $T \gtrsim 0.7$ K), the instabilities appear to be governed by the Donnelly number and collapse, hence they must originate in the normal fluid component. On the contrary, at low temperatures, the governing parameter is the paddle's velocity, therefore the instabilities are of the Donnelly-Glaberson type and originate in the superfluid component. It seems therefore that there is, within the covered temperature range, a cross-over of first instability which at low temperatures originates from the superfluid component while at higher temperatures from the normal component. We

shall argue below that this behavior is easily observed also in the drag data from the flow due to the torsionally oscillating disc.
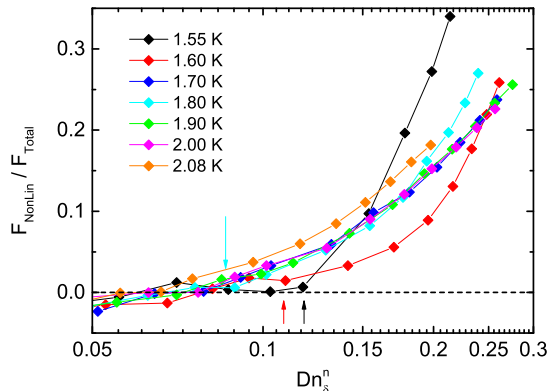


FIG. 13. Normalized non-linear damping force as a function of the Donnelly number of the silicon double-paddle. At higher temperatures, the non-linear damping is temperature independent and any deviation from this universal dependence is due to the contribution of the superfluid component. The black, read and cyan arrows indicate the Donnelly number where non-linear damping sets in at 1.55, 1.60 and 1.80 K, respectively.

## D. Torsionally Oscillating Disc

Since we are mainly interested in the analysis of the non-linear drag forces acting on the disc, the linear part of the lower plot in Fig. 5, which describes the viscous decay due to laminar flow, was fitted by a straight line, which was then withdrawn from the logarithms of the signal maxima. The fitting range was selected manually to avoid any influence from the noise at late times (low amplitudes).

We define a drag coefficient for a thin disc torsionally oscillating in a viscous fluid as

$$C_D = \frac{2\Gamma}{A\rho\Omega_0^2 R^3} , \qquad (7)$$

where $\Gamma = \pi R^4 \sqrt{\eta\rho\omega/2}$ is the damping coefficient, $R$ is the disc's radius, $A = \pi R^2$ is the surface area of the top (or bottom) of the disc, $\Omega_0$ is the amplitude of the angular velocity and $\omega$ is the angular frequency of oscillation. For a rationale of this definition, we refer the reader to Appendix A. We plot the drag coefficient $C_D$ against the angular amplitude of the disc oscillations measured at various temperatures in Fig. 14. As expected, there is no collapse of $C_D$ at small angular amplitudes of oscillation.

In order to achieve universal scaling at low amplitudes of oscillation, in the same virtue as for other vibrating objects above, we define the normal fluid drag coefficient
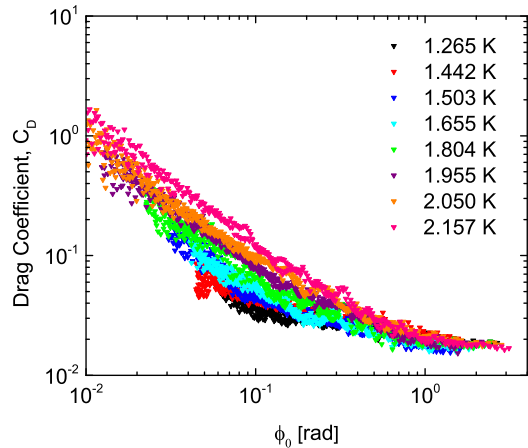


FIG. 14. Drag coefficient $C_D$ as a function the angular amplitude of oscillation for the torsionally oscillating disc at various temperatures.
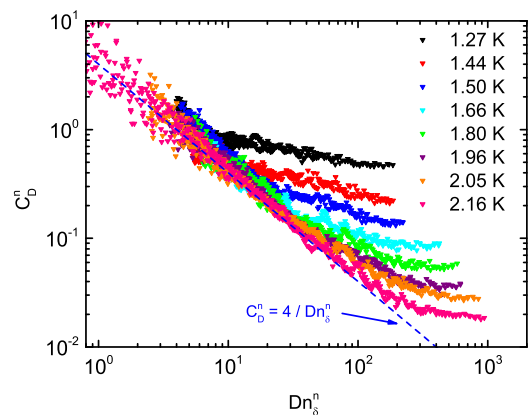


FIG. 15. Normal fluid drag coefficient as a function of the Donnelly number for the torsional disc at the various indicated temperatures. The blue dashed line is the predicted dependence from viscous drag theory.

as

$$C_D^n = \frac{2I\alpha}{\pi A\rho_N R^3\phi_0} = \frac{2M_F}{SR^3\rho_n\omega^2} \simeq \frac{\rho h\alpha}{\pi\rho_N R\phi_0}, \qquad (8)$$

where and $M_F$ is the moment of the dissipative forces, $S = \pi R^2$ is the area of the relevant surface of the torsional oscillator. Here, $\alpha$ is the logarithmic decrement $(2\alpha_i = ln(\phi_{i-1}) - ln(\phi_{i+1}))$ obtained from the signal, $R$ represents the disc radius, $h$ its height, and $I$ stands for its moment of inertia. In Fig. 15, we plot the normal fluid drag coefficient $C_D^n$ as a function of the boundary layer based Reynolds number, i.e., the Donnelly number, $Dn = \rho_N \delta_N R\omega\phi_0/\eta$). We again refer the reader to Appendix A for details of this approach.

Fig. 15 shows that for low Donnelly numbers $Dn$ the viscous drag $C_D^n$ reasonably collapses to a single depen-
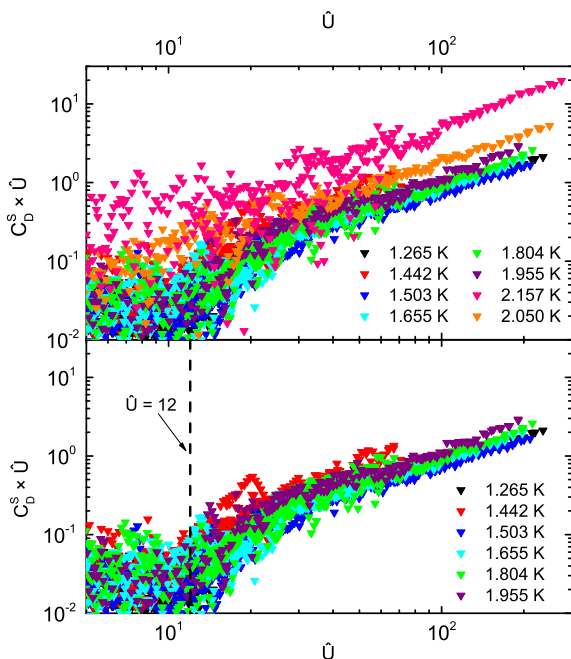
FIG. 16. Product of the disc's non-linear superfluid drag co-efficient and dimensionless velocity as a function of the dimensionless velocity at various temperatures. Below about 1.955 K, the viscous drag acting on the disc collapses to a single dependence, but the instability is not described in terms of classical fluid dynamics as shown in the bottom panel.

dence. One would naturally expect the drag coefficient to follow a $1/\phi_0$, i.e., the inverse velocity dependence in laminar normal fluid flow, the more that the situation differs here in that the superfluid component remains stationary in the laboratory frame of reference, similarly as in the famous experiment of Andronikashvili [21]. On the other hand, the instabilities clearly displayed in Fig. 15 are not characterized by any single value of $Dn$. This implies that the instability cannot be generally explained by viscous fluid dynamics of the normal fluid and must must be somehow related to the superfluid component. Therefore, we need to concentrate on the non-linear contribution of the drag forces acting on the disc due to the superfluid component. To this end, we will now discuss the flow of He II due to the torsionally oscillating disc in terms of dimensionless velocity defined as $\hat{U} = R\omega\phi_0/\sqrt{\kappa\omega}$.

Using the same logic as we used above to define $C_D^n$, we now define the superfluid drag coefficient as

$$C_D^s = 2I\alpha\pi A\rho_S R^3\phi_0 \simeq \rho h\alpha/\pi\rho_S R\phi_0. \tag{9}$$

The drag coefficient $C_D^s$ must remain about zero until some critical **velocity** $\hat{U}_C$ where quantized vorticity becomes formed and some of the quantized vortices will reconnect to generate vortex loops which will propagate into the bulk superfluid, carrying with them some of the kinetic energy supplied by the oscillating disc. This process is experimentally observed as an increase in the drag

coefficient $C_D^s$, which is plotted (after eliminating laminar drag contribution) as a function of the dimensionless velocity $\hat{U}$ in Fig. 16. In the top panel, which shows no collapse of the data, we plot all our data, obtained at various temperatures. The situation is very different if only the data taken at 1.955 K and below are displayed, see the bottom panel of Fig. 16, where one observes a distinct critical value of the dimensionless velocity $\hat{U}_c \approx 12$. At these temperatures, the initial instability is most likely related to the production of quantized vorticity by a Donnelly-Glaberson type instability (vortex loop self-reconnection), since the non-linear contribution is temperature-independent, showing that the superfluid component undergoes the transition alone, while the normal component flow remains laminar. The bahavior of the data above 1.955 K suggests that the normal fluid component may also become unstable above $\hat{U} \approx 100$. Indeed, the normal fluid fraction becomes significant at these temperatures, its kinematic viscosity $\nu_n = \eta/\rho_n$ decreases and the Donnelly number controlled instability in the normal fluid occurs at these higher temperatures earlier than the Donnelly-Glaberson type instability in the superfluid component. Mutual friction then tends to couple the normal and superfluid velocity fields together, until eventually He II (at quasiclassical scales) behaves as a single component fluid possessing an effective kinematic viscosity. In the limit of very large velocities the drag ought to become velocity-independent, in the same virtue as in classical viscous fluids.

## V. DISCUSSION

### A. Two-fluid Regime

Let us generalize the described above experimental results on the two fluid He II flows due to several types of oscillators. In all of them the normal fluid flow is characterized by high Stokes number, and for low velocities it is laminar. In this limit the superflow is either (almost) potential or, in the case of torsionally oscillating disc, the superfluid component remains (almost) stationary in the laboratory frame of reference. Here almost means that there always exist remnant quantized vortices, whose density can be estimated based on the work of Awschalom, Milliken and Schwarz [59]. We therefore have two (almost) independent velocity fields and flows of the normal and superfluid components can be treated independently.

It is therefore natural to treat, in this limit, the normal fluid as classical viscous fluid and not at all surprising that the drag coefficient $C_D^N$ due to the normal fluid displays universal inverse scaling in terms of the Donnelly number $Dn$. Assuming that the superfluid component remains potential, upon increasing the Donnelly number the universal scaling holds and describes instabilities in the normal flow leading to gradual transition from laminar to turbulent drag regime in the normal flow. The

normal fluid flow is no longer laminar and the overall He II flow can loosely be characterized as quantum turbulence, despite there are (almost) no quantized vortices in the flow. In some cases, the opposite situation appears in that the critical velocity associated with the Glaberson-Donnelly instability in the superfluid comes first, before instability in the normal fluid flow. This situation is not new in superfluid hydrodynamics. Indeed, in experiments with superfluid $^3$He-B the thick normal component virtually does not move in the laboratory frame of reference. Still, below about half of the critical temperature $T_c$ the dissipative mutual friction coefficient falls below unity and a tangle of quantized vortices - superfluid turbulence - can exist in the soup of thick stationary normal fluid. In He II the situation is different in that the quantized vorticity coexists with the laminar boundary layer flow of the thin normal component. This situation is reported, to the best of our knowledge, for the first time and is best illustrated for the case of He II flow due to the torsionally oscillating discs at low temperatures (below about 1.9 K in this particular case).

Now, as the Glaberson-Donnelly instability occurs upon reaching a critical velocity, but the instability in the normal fluid flow is governed upon reaching a critical Donnelly number, a crossover is possible, thanks to the steep temperature dependence of the kinematic viscosity of the normal fluid. In other words, in our particular example of He II flow due to the torsionally oscillating disc, at high temperatures - closer to the superfluid transition temperature $T_\lambda$ the classical instability in the normal fluid is reached first, while at low temperatures the situation is reversed in favor of the Donnelly-Glaberson instability. The existence of this crossover, observed also in the flow due to double-paddle oscillator, is reported for the first time and is quite remarkable. Either instability eventually serves as a trigger for the other one, mediated by the mutual friction force, until in the limit of high velocities, both fluids are tightly coupled in the vicinity of the oscillator and He II behaves as a single-component quasiclassical fluid.

### B. Ballistic Regime

Below approximately 0.7 K, however, He II can no longer be described by the continuum two-fluid model, because the density of thermal excitations making up the normal component is so low, that (given the typical size of cryogenic experiments) excitation-wall interaction becomes dominant with respect to excitation-excitation scattering processes. This effect was observed, e.g., with vibrating wires [35], or spheres [22]. In the absence of quantum turbulence, superfluid helium is then best described as a dilute gas of ballistically propagating thermal excitations in the superfluid component, which itself acts only as a physical vacuum. It is therefore natural, to seek analogy with classical dilute gases and compare the experimental results obtained with oscillators in both types of fluids. To make a direct comparison possible, we seek to define the pressure, mean free path and relaxation time of the thermal excitations, as these are the fundamental quantities used to interpret the data from classical fluids [6–9].

The dispersion relation of thermal excitations in $^4$He has been suggested by Landau [16], and later verified in neutron diffraction experiments [60]. Long-wave excitations correspond to sound quanta and are called phonons, while excitations with higher momenta located around a minimum in the dispersion relation are traditionally called rotons. Statistical description of thermal excitations in $^4$He is usually carried out by considering phonons and rotons separately, ignoring excitations with higher energies due to their low occupation densities. Phonons are then approximately described by a linear dispersion relation $\epsilon_{ph} = cp$, where $\epsilon_{ph}$ is phonon energy, $c$ is the (first) sound velocity, and $p$ is momentum, while roton energies follow $\epsilon_{rot} = \Delta + (p - p_0)^2/(2m_r)$, where $\Delta$ is the roton minimum gap, $p_0$ the roton momentum and $m_r$ the roton effective mass.

Approximations of phonon and roton pressures can be obtained from a statistical description of both types of excitations as (non-interacting) ideal Bose gases [61]. The pressures are defined from a grand canonical treatment of a Bose-Einstein condensate (with zero chemical potential) as $p = -k_B T \frac{\partial ln(Z)}{\partial V}$, where $k_B$ is the Boltzmann constant, $T$ the thermodynamic temperature and the grand partition function $Z$ is given in Thomas-Fermi approximation as:

$$ln(Z) = -\int_0^\infty \frac{d^3\boldsymbol{p}}{(2\pi\hbar)^3} ln(1 - e^{-\epsilon/k_B T}). \qquad (10)$$

Phonon and roton pressures are obtained by substituting $\epsilon_{ph}$ or $\epsilon_{rot}$ for $\epsilon$; integration from zero to infinity instead of the corresponding ranges of energies/momenta produces negligible errors as the high energy states are again statistically insignificant. For rotons, one may use Maxwell statistics instead of Bose statistics if $T \ll \Delta \approx 8.6$ K and an additional assumption $T \ll p_0^2/m_r$ is necessary [61], which is satisfied automatically if the first one holds. Thus for temperatures below $\approx 1.5$ K, we obtain with sufficient accuracy the phonon and roton pressures:

$$P_{ph} = \frac{\pi^2 (k_B T)^4}{90 c^3 \hbar^3}, \qquad (11)$$

$$P_{rot} = \sqrt{\frac{m_r}{2\pi^3}} p_0^2 T^{3/2} e^{-\Delta/T}. \qquad (12)$$

The computed excitation pressures along with the saturated vapor pressure are plotted against temperature in Fig. 17.

The distributions of thermal excitations follow a kinetic equation of the Boltzmann type, with collision integrals determined by the relevant quantum scattering processes. Apart from these, processes corresponding to excitation emission and absorption must be taken into account as well [61]. The mean free paths and relaxation
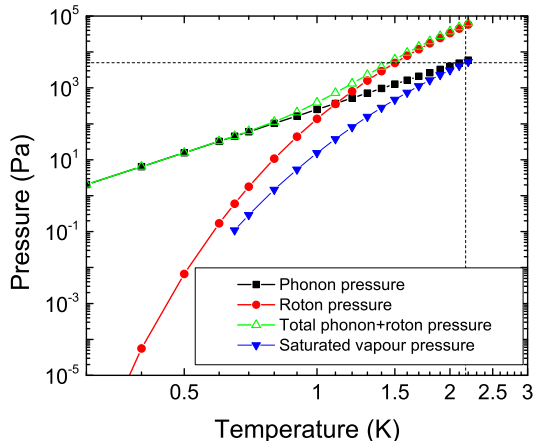
FIG. 17. Phonon and roton pressures compared to the saturated vapor pressure in He II. The dashed lines mark the pressure and temperature corresponding to the superfluid phase transition – the lambda point. Interesting connections between thermal excitations and evaporation exist in He II, which are beyond the scope of this work [62].

times are thus significantly more challenging to define precisely, as they depend on exact details of various types of multi-excitation processes occurring in He II. Analytical expressions for relaxation times may be derived approximately only for particular scattering processes [63], while a complete description remains impossible without intensive numerical calculations.

At temperatures below $\approx 0.6$ K, the situation is greatly simplified, as the roton density becomes so low that rotons cease to affect the behavior of He II in a statistically significant manner and may be neglected. Limiting ourselves to temperatures below 0.6 K and phonon excitations only, analytical treatment becomes possible [63] and has been tested by experiments with vibrating wires [35]. The most important types of scattering events in this temperature region are three-phonon processes (3pp) and four-phonon processes (4pp). For a detailed discussion, we refer the reader to Ref. 64 and other notable works on the topic [65, 66]. We will use the results of Ref. 64 that are in agreement with the experiments of Greywall [49] and of the Kharkov laboratory [67] and use them to establish a temperature-dependent phonon relaxation time $\tau_{ph}$ and mean free path $\lambda_{ph} = \tau_{4ph}c$, where $c$ is the first sound velocity. At temperatures between 0.2 K and 1.0 K, the mean free path of Ref. 64 may be approximated with sufficient precision as:

$$log_{10}(\lambda[m]) = a_0 + a_1 T + a_2 T^2 + a_3 T^3 + a_4 T^4, \quad (13)$$

with $T$ in kelvin and the coefficients given as $(a_0, a_1, a_2, a_3, a_4) = (3.829, -26.37, 35.86, -25.17, 6.862)$. This corresponds to curve (1) in Fig. 2 of Ref. 64.

Temperature-dependent phonon Knudsen and Weissenberg numbers may be obtained from their usual defini-

tions $\text{Kn}_{ph} = \lambda_{ph}/L$, $\text{Wi}_{ph} = \omega\tau_{ph}$. These dimensionless parameters are plotted in Fig. 18 against temperature for $L = 75$ $\mu$m and $f = 6.4$ kHz and 40.0 kHz, which corresponds to the 6.4 kHz tuning fork oscillating in its fundamental mode and first overtone, respectively, showing the importance of the ballistic treatment below $\approx 0.7$ K and of non-equilibrium description at lower temperatures. Note that we consider the Knudsen and Weissenberg numbers well-defined only for $T < 0.6$ K, as discussed above. A rigorous treatment of higher temperatures would require a full-fledged quantum-mechanical molecular dynamics simulations of thermal excitations in He II, which represent in themselves an interesting and developing topic of research. We hope that this work will stimulate interest in the microscopic description of superfluid helium and lead to a better understanding of the fundamental processes involved.
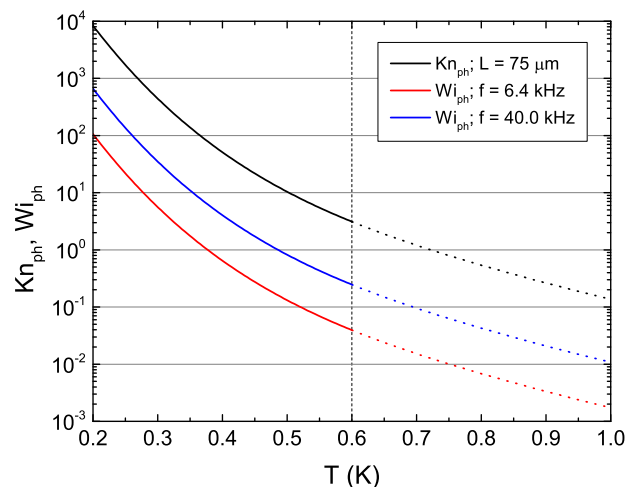


FIG. 18. Phonon Knudsen number (for $L = 75$ $\mu$m) and Weissenberg numbers (for $f = 6.4$ kHz and 40.0 kHz) plotted against temperature. The dashed line separates the interval of temperatures $T < 0.6$ K, where the properties of He II are reliably described by phonon scattering processes only (solid lines), from the range, where the dynamics of He II might become influenced by the presence of rotons, leading to increasing rates of phonon-roton scattering and deviations from the presented dependences (dotted lines).

## VI. CONCLUSIONS

We have performed systematic measurements of high Stokes number flows of He II due to oscillatory motion of selected oscillators: vibrating wire resonator, tuning fork, double-paddle, and torsionally oscillating disc, over a broad temperature range where our working fluid, He II, displays the two-fluid behavior. We have shown that in this class of flow the origin of any instability in the normal or superfluid component can be determined by complex drag force analysis, based on which one can sep-

arate the drag offered to these oscillators by the normal and superfluid components of He II. For low velocities, we observe **universal viscous drag scaling** in terms of the suitably defined drag coefficient $C_D^n$ and the normal fluid boundary layer-based Reynolds number which we call the Donnelly number $Dn$.

The superfluid component does not contribute to the drag until an instability associated with extrinsic production of quantized vorticity occurs, governed by the dimensionless **velocity** $\hat{U} = U/\sqrt{\kappa\omega}$. The underlying physics involves Donnelly-Glaberson instability, i.e., self-reconnections of quantized vortices upon reaching a critical velocity. Until then the flow of the superfluid component is either potential (almost, except remnant vorticity) with the superfluid component playing a role of a physical vacuum, re-normalizing the hydrodynamic effective mass of the oscillators, or (in the case of the torsionally oscillating disc) the superfluid component remains stationary in the laboratory frame of reference.

Which instability (i.e., classical hydrodynamic instability of laminar flow of the normal component or Donnelly-Glaberson instability in the superfluid component) occurs first depends both on the geometry of the oscillator and temperature. We observe a crossover between them, thanks to the steep temperature dependence of the kinematic viscosity of the normal fluid. Upon increasing velocity, either instability can live on its own until eventually it serves as a trigger for the other one, mediated by the mutual friction force. In the limit of high velocities, both fluids are tightly coupled in the vicinity of the oscillator and He II behaves as a single-component quasiclassical fluid.

Additionally, at temperatures below 1 K, a transition to a ballistic regime of the normal component flow occurs in He II and we develop a formalism allowing direct comparison between measurements with resonators in He II and (nanomechanical) oscillators in classical dilute gases.

### Appendix A: Hydrodynamic Description of the Torsionally Oscillating Disc

The motion of the linear harmonic torsional oscillator is given by the equation:

$$I_0\ddot{\phi} + \kappa\phi = M_E \tag{A1}$$

where $\phi$ is the angular displacement, $I_0$ is the moment of inertia, $\kappa$ is the moment of torsion of the fiber and $M_E$ represents the sum of all external moments of force acting on the axis of the torsional oscillator, including frictional forces from the surrounding liquid, $M_F$.

In laminar flow, with some simplification, the momentum of the frictional forces can be calculated on the basis of the analytical resolution of the N-S equations.

First, we assume that the velocity profile $\boldsymbol{u}(\boldsymbol{r}, t)$ corresponds to the rotation of the rigid body modulated with the distance from the disc, $\boldsymbol{u}(\boldsymbol{r}, t) = \boldsymbol{\Omega}(z, t) \times \boldsymbol{r}$, where $\boldsymbol{\Omega}(z, t) = (0, 0, \Omega(z, t))$, in which $\Omega(z, t)$ is the instantaneous rotational speed of the fluid at the distance $z$ from the disk surface. Furthermore, we assume that the diameter of the disc $R$ is greater than its thickness $h$ and also that it has a Stokes viscous boundary layer $\delta = \sqrt{2\nu/\omega}$, where $\nu$ is the kinematic viscosity of the fluid and $\omega$ is the angular frequency. The N-S equation is then expressed in the form:

$$\frac{\partial\Omega(z, t)}{\partial t} = \nu\frac{\partial^2\Omega(z, t)}{\partial z^2} \tag{A2}$$

Harmonic solutions of this equation meeting the boundary conditions on the surface of the disc ($z = 0$) and at infinity has the form

$$\Omega(z, t) = \Omega_0 e^{-z/\delta}e^{i(\omega t - z/\delta)}, \tag{A3}$$

where $\Omega_0$ is the instantaneous amplitude of the disk's angular velocity.

The total torque of the forces acting on the disk will be determined by integration of both disc surfaces. The magnitude of the local viscous torsional force $F_v$ (per unit area) is given by $F_v(r, t) = \eta\frac{\partial u(z,t)}{\partial z}$, where $\eta$ is the dynamic fluid viscosity. The magnitude of the local contribution to the torque of the resistive forces is then given as $M_v(r, t) = rF_v(r, t)$. The total moment of frictional forces is given as:

$$\begin{aligned} M_F(t) &= 2\int_0^{2\pi}\int_0^R M_v(r, t)r\,d\theta\,dr \\ &= -4\pi\eta\frac{1+i}{\delta}\Omega_0 e^{i\omega t}\int_0^R r^3\,dr \\ &= -\pi\eta\frac{1+i}{\delta}\Omega_0 R^4 e^{i\omega t} \end{aligned} \tag{A4}$$

For a disk which behaves as a damped harmonic oscillator, $\phi(t) = \phi_0(t)e^{i\omega t}$. The angular velocity will be given as $\Omega(t) = \partial\phi/\partial t$, which for a damped oscillator reduces to $\Omega(t) \approx i\omega\phi_0(t)e^{i\omega t}$. The amplitude of the disc's angular velocity can therefore be expressed as $\Omega(t) \approx i\omega\phi_0(t)$. After inserting $\delta = \sqrt{2\nu/\omega}$, we get the resulting moment of the frictional forces:

$$M_F(t) = \frac{\pi}{\sqrt{2}}(1-i)\sqrt{\eta\omega\rho}\,\omega R^4\phi_0 e^{i\omega t} \tag{A5}$$

The moment of the friction forces is therefore phase-shifted with respect to the angular velocity of the disk

by $\pi/4$ (see factor 1-i). By defining a hydrodynamically induced moment, the inertia $I_{HD} = \pi R^4 \sqrt{\eta\rho/2\omega}$ and the damping coefficient $\Gamma = \pi R^4 \sqrt{\eta\rho\omega/2}$, we can describe the moment of the frictional forces as:

$$M_F(t) = -\Gamma\dot{\phi} - I_{HD}\ddot{\phi}. \qquad (A6)$$

After we substitute A6 into the dynamic equation of motion A1 we get:

$$I\ddot{\phi} + \Gamma\dot{\phi} + \kappa\phi = 0, \qquad (A7)$$

where $I = I_0 + I_{HD}$ is the total effective moment of inertia of the disk and surrounding fluid. After dividing by the moment of inertia $I$, we obtain:

$$\ddot{\phi} + 2\gamma\dot{\phi} + \omega_0^2\phi = 0, \qquad (A8)$$

where $\gamma = \Gamma/2I$ the effective damping coefficient, and $\omega_0^2 = \kappa/I$ is the intrinsic angular frequency of the undamped resonator squared. Thus, we have a standard equation of the damped harmonic oscillator:

$$\phi(t) = \phi_0 e^{-\gamma t} e^{i\omega t}, \qquad (A9)$$

where the angular frequency $\omega$ is related to the frequency of an undamped oscillator according to the relation $\omega^2 = \omega_0^2 - \gamma^2$

By processing the disk videos, we obtain data in the form of $\phi(t)$, from this, we determined the extrema $\phi_n$ and their corresponding time values $t_n$ for a total of N oscillations.

Now, we will show how to make since of these physical data of these data. For every time $t_n$ (except for n = 1 and n = N) we can determine the logarithmic decrement $\alpha_n = \ln(\phi_{n-1}) - \ln(\phi_{n+1})$ and the oscillation period $T_n = t_{n+1} - t_{n-1}$. The angular frequency is given as $\omega_n = 2\pi/T_n$. The effective damping coefficient $\gamma$ is then expressed as $\gamma_n = \alpha_n/T_n$. The frequency of the damped oscillator $\omega_0$ is determined from the relationship $\omega_{0n}^2 = \omega_n^2 + \gamma_n^2$ and the corresponding period for a damped oscillator is $T_{0n} = 2\pi/\omega_{0n}$.

In addition to these purely mechanical quantities, it is appropriate to define some hydrodynamic quantities. The resistive in-line force $F$ for a body experiencing a flow is given by $F = \frac{1}{2}C_D A\rho U^2$, where $C_D$ is the dimensionless drag coefficient, $A$ is the cross section of the body perpendicular to the direction of motion, $\rho$ is the density of the fluid and $U$ is the (homogenous) velocity of the fluid. By analogy with Newton's Law it is possible to define the damping coefficient for the torsionally oscillating disk as:

$$\frac{\Gamma\Omega_0}{R} = \frac{1}{2}C_D A\rho\Omega_0^2 R^2, \qquad (A10)$$

where $A$ is the disc's surface area $(A = \pi R^2)$ instead of the area perpendicular to the flow. From which we therefore get the drag coefficient:

$$C_D = \frac{2\Gamma}{A\rho\Omega_0^2 R^3} = \frac{4I\gamma}{A\rho\Omega_0^2 R^3} = \frac{2I\alpha}{\pi A\rho R^3\phi_0}. \qquad (A11)$$

If the hydrodynamic contribution is negligible, the moment of inertia for the disc is $I_0 = \frac{1}{2}mR^2$, where the mass of the disc can be expressed as $m = Ah\rho_D$. This can be further simplified as:

$$C_D = \frac{1}{\pi}\frac{\rho_D h\alpha}{\rho R\phi_0}. \qquad (A12)$$

It is desirable to define a dimensionless parameter describing the flow, e.g. Reynolds's number.

To this end, we will assume that the characteristic velocity is $U = R\omega\phi_0$. If we assume the characteristic dimension is the radius of the disc $R$, we have $Re_R = R^2\omega\phi_0/\nu$ or $Re_\delta = \delta R\omega\phi_0/\nu$ if we assume that the characteristic dimension is the viscous penetration depth. Next, we define the Stokes parameter as

$$\beta = \frac{\omega R^2}{2\pi\nu} = \frac{1}{\pi}\frac{R^2}{\delta^2}. \qquad (A13)$$

Up this point, we have been working within the confides of classical fluid dynamics. Because we are working within the two-fluid model of superfluid helium, the definition of some of the variables can be redefined to describe flow due to the normal or superfluid component. For the laminar potential flow in the superfluid component, the will be no fluid displacement and hence no change in the equation of motion. For the normal fluid component's contribution for example, (indicated by the lower index N) the density of the whole fluid $\rho$ will be replaced by the density of the normal component $\rho_N$, the effective kinematic viscosity $\nu$ will be replaced by $\eta/\rho_n$, and in the definition of $Re_\delta$ and $\beta$, $\delta$ will be replaced by $\delta_N = \sqrt{2\nu/(\omega\rho_N)}$.

[1] G. G. Stokes, *Transactions of the Cambridge Philosophical Society*, Vol. VIII. Part I, 105 (1843).
[2] G. H. Keulegan, L. H. Carpenter, *J. of Research of the Natl. Bureau of Standards* **60**, 423 (1958).
[3] Chang-Yi Wang, *J. Fluid Mech.* **32**, 55 (1968).
[4] T. Sarpkaya, *J. Fluid Mech.*, **165**, 61 (1986).

[5] M. Tatsuno, P. W. Bearman, *J. Fluid Mech.* **211**, 157 (1990).

[6] K. L. Ekinci, D. M. Karabacak, and V. Yakhot, *Phys. Rev. Lett.* **101**, 264501 (2008).

[7] K. L. Ekinci, V. Yakhot, S. Rajauria, C. Colosquiac and D. M. Karabacak, *Lab Chip* **10**, 3013 (2010).

[8] E. C. Bullard, Jianchang Li, C. R. Lilley, P. Mulvaney, M. L. Roukes, and J. E. Sader, *Phys. Rev. Lett.* **112**, 015501 (2014).

[9] M. Defoort, K. J. Lulla, T. Crozes, O. V. Maillet, O. Bourgeois, and E. Collin, *Phys. Rev. Lett.* **113**, 136101 (2014).

[10] R. J. Donnelly and C. F. Barenghi, *J. Phys. Chem. Ref. Data* **27**, 1217 (1998).

[11] S. Fuzier, B. Baudouy and S. W. Van Sciver, *Cryogenics* **41**, 453 (2001).

[12] B. Saint-Michel, E. Herbert, J. Salort, C. Baudet, M. Bon Mardion, P. Bonnay, M. Bourgoin, B. Castaing, L. Chevillard, F. Daviaud, P. Diribarne, B. Dubrulle, Y. Gagne, M. Gibert, A. Girard, B. Hébral, Th. Lehner, B. Rousset, and SHREK Collaboration, *Phys. Fluids* **26**, 125109 (2014).

[13] J. J. Niemela, L. Skrbek, K. R. Sreenivasan, and R. J. Donnelly, *Nature* **404**, 837 (2000).

[14] R. D. McCarty, *Thermophysical properties of helium-4 from 2 to 1500 K with pressures to 1000 atmospheres,* Technical Note 631, National Bureau of Standards, Gaithersburg, MD (1972).

[15] V. D. Arp and R. D. McCarty, *The properties of critical helium gas,* Technical Report, University of Oregon, Eugene, OR (1998).

[16] L. D. Landau, *J. Phys. (USSR)* **5**, 71 (1941); *J. Phys. (USSR)* **11**, 91 (1947).

[17] R. J. Donnelly, *Quantized Vortices in Helium II* (Cambridge University Press, Cambridge, 1991).

[18] C. F. Barenghi, L. Skrbek and K. R. Sreenivasan, *Proc. Natl. Acad. Sci. U.S.A.* **111**, 4647 (2014).

[19] A. C. Hollis-Hallett, *Proc. Roy. Soc. London. Series A*, **210**, 404 (1952).

[20] R. J. Donnelly, A. C. Hollis-Hallett, *Annals of Phys.* **3**, 320 (1958).

[21] E. L. Andronikashvili, *J. Phys. (Moscow)* **10**, 201 (1946).

[22] J. Jäger, B. Schuderer, and W. Schoepe, *Physica B* **210**, 201 (1995).

[23] M. Niemetz, W. Schoepe, *J. Low Temp. Phys.* **135**, 447 (2004).

[24] J. Luzuriaga, *J. Low Temp. Phys.* **108**, 267 (1997).

[25] H. A. Nichol, L. Skrbek, P. C. Hendry, P. V. E. McClintock, *Phys. Rev. Lett.* **92**, 244501 (2004).

[26] H. A. Nichol, L. Skrbek, P. C. Hendry, P. V. E. McClintock, *Phys. Rev. E* **70**, 056307 (2004).

[27] P. Švančara, M. La Mantia, *J. Fluid Mech.*, **832**, 578 (2017).

[28] R. Blaauwgeers, M. Blažková, M. Čovečko, V. B. Eltsov, R. de Graaf, J. J. Hosio, M. Krusius, D. Schmoranzer, W. Schoepe, L. Skrbek, P. Skyba, R.E. Solntsev, D.E. Zmeev, *J. Low Temp. Phys.* **146**, 537 (2007).

[29] D. Garg, V. B. Efimov, M. Giltrow, P. V. E. McClintock, L. Skrbek, W. F. Vinen, *Phys. Rev. B* **85**, 144518 (2012).

[30] S.L. Ahlstrom, D.I. Bradley, M. Čovečko, S.N. Fisher, A.M. Guénault, E.A. Guise, R.P. Haley, O. Kolosov, P.V.E. McClintock, G.R. Pickett, M. Poole, V. Tsepelin, and A.J. Woods, *Phys. Rev. B* **89**, 014515 (2014).

[31] D. Schmoranzer, M.J. Jackson, V. Tsepelin, M. Poole, A.J. Woods, M. Čovečko, and L. Skrbek, *Phys. Rev. B* **94**, 214503 (2016).

[32] E. N. Martinez, P. Esquinazi, J. Luzuriaga, American *J. of Physics* **58**, 1163 (1990).

[33] D. Duda, P. Švančara, M. La Mantia, M. Rotter, L. Skrbek, *Phys. Rev. B* **92**, 064519 (2015).

[34] W. F. Vinen, *Proc. Roy. Soc. London. Series A*, **181**, 1524 (1961).

[35] M. Morishita, T. Kuroda, A. Sawada, and T. Satoh, *J. Low Temp. Phys.*, **76**, 387 (1989).

[36] D.I. Bradley, D.O. Clubb, S.N. Fisher, A.M. Guénault, R.P. Haley, C.J. Matthews, G.R. Pickett and K.L. Zaki, *J. Low Temp. Phys.* **138**, 493 (2005).

[37] R. Goto, S. Fujiyama, H. Yano, Y. Nago, N. Hashimoto, K. Obara, O. Ishikawa, M. Tsubota, and T. Hata, *Phys. Rev. Lett.* **100**, 045301 (2008).

[38] L. Skrbek and W. F. Vinen, *The use of vibrating structures in the study of quantum turbulence,* in Progress in Low Temperature Physics edited by M. Tsubota and W. P. Halperin (Elsevier, Amsterdam, 2009), Vol. XVI, Chap. 4.

[39] L. Skrbek and W. F. Vinen, *Proc. Natl. Acad. Sci. U.S.A.*, **111**, 4699 (2014).

[40] C.L. Spiel, R.O. Pohl, A.T. Zehnder, *Rev. Sci. Instrum.* **72**, 1482 (2001).

[41] E. Zemma and J. Luzuriaga, *J. Low Temp. Phys.* **166**, 171 (2012).

[42] D. Schmoranzer, M. Jackson, E. Zemma and J. Luzuriaga, *J. Low Temp. Phys.* **187**, 482 (2017).

[43] J.C. Wheatley, O.E. Vilches, and W.R. Abel, *J. Low Temp. Phys.* **4**, 1 (1968).

[44] D. D. Holm in *Quantized Vortex Dynamics and Superfluid Turbulence. Lecture Notes in Physics* **571**, edited by C.F. Barenghi, R.J. Donnelly and W.F. Vinen (Springer, Berlin, Heidelberg, 2001).

[45] In honor and memory of Russell J. Donnelly, who for the first time suggested using this dimensionless parameter, a "Reynolds number" based on the viscous penetration depth defined for the normal component of He II only, in his joint publication with A. C. Hollis-Hallett in 1958 [20].

[46] W. I. Glaberson, W. W. Johnson and R. M. Ostermeier, *Phys. Rev. Lett.* **33**, 1197 (1974).

[47] M. Blažková, D. Schmoranzer, L. Skrbek, and W. F. Vinen, *Phys. Rev. B* **79**, 054522 (2009).

[48] D. Benin and H. J. Maris, *Phys. Rev. B* **18**, 3112 (1978).

[49] D. S. Greywall, *Phys. Rev. B* **23**, 2152 (1981).

[50] D. I. Bradley, M. Čovečko, S. N. Fisher, D. Garg, E. Guise, R.P. Haley, O. Kolosov, G. R. Pickett, V. Tsepelin, D. Schmoranzer, and L. Skrbek, *Phys. Rev. B* **85**, 014501 (2012).

[51] D. Schmoranzer, M. La Mantia, G. Sheshin, I. Gritsenko, A. Zadorozhko, M. Rotter, L. Skrbek, *J. Low Temp. Phys.* **163**, 317-344 (2011).

[52] D. I. Bradley, M. J. Fear, S. N. Fisher, A. M. Gunault, R. P. Haley, C. R. Lawson, P. V. E. McClintock, G .R. Pickett, R. Schanen, V. Tsepelin, L. A. Wheatland, *J. Low Temp. Phys.* **156**, 116 (2009).

[53] A. M. Guénault, C. J. Kennedy, S. G. Mussett and G. R. Pickett, *J. Low Temp. Phys.* **62**, 511 (1986).

[54] K. J. Strnat, D. Li, and H. Mildrum, *High and Low Temperature Properties of Sintered Nd-Fe-B Magnets*, paper no. VIII-8 at the 8th Int. Workshop on Rare Earth Magnets and Their Applications, Dayton, OH, 6-8 May

(1985); T. Hara, T. Tanaka, H. Kitamura, *et al., Phys. Rev. Accel. Beams*, **7**, 050702 (2004).

[55] K. Karrai and R. D. Grober in *Near-Field Optics*, edited by M. A. Paesler and P. T. Moyer, *Proc. SPIE* **2535**, 69 (1995).

[56] S. Holt, P. Skyba, *Rev. Sci. Instrum.* **83**, 064703 (2012).

[57] L. D. Landau and E. M. Lifshitz, *Fluid Mechanics*, Pergamon Press, London (1959).

[58] D. I. Bradley, P. Crookston, M. J. Fear, S. N. Fisher, G. Foulds, D. Garg, A.M. Guénault, E. Guise, R. P. Haley, O. Kolosov, G. R. Pickett, R. Schanen and V. Tsepelin, *J. Low Temp. Phys.* **161**, 536 (2010).

[59] D. D. Awschalom, F. P. Milliken, and K. W. Schwarz, *Phys. Rev. Lett.* **53**, 1372 (1984).

[60] J. L. Yarnell, G. P. Arnold, P. J. Bendt, and E. C. Kerr, *Phys. Rev.* **113**, 1379 (1959).

[61] I. M. Khalatnikov, *An Introduction to the Theory of Superfluidity*, Westview Press, CO (2000).

[62] D.S. Hyman, M.O. Scully, A. Widom, *Phys. Rev.* **186**, 1 (1969).

[63] L. D. Landau, I. M. Khalatnikov, *Zh. Eksp. Teor. Fiz.* **19**, 637, 709 (1949), also Collected Papers of L. D. Landau, D. Ter Haar, ed. (Pergamon, Oxford, 1965), p. 494.

[64] I. N. Adamenko, Yu. A. Kitsenko, K. E. Nemchenko, A. F. G. Wyatt, *Low Temp. Phys.* **35**, 198 (2009).

[65] H. J. Maris, *Phys. Rev. Lett.* **28**, 277 (1972), H. J. Maris, *Phys. Rev. A* **8**, 1980 (1973).

[66] D. Benin, *Phys. Rev. B* **11**, 145 (1975).

[67] A. A. Zadorozhko, G. A. Sheshin, E. Ya. Rudavskii, V. K. Chagovets, Yu .A. Kitsenko, *Fiz. Nizk. Temp.* **35**, 134 (2009).

[68] S. Babuin, M. Stammeier, E. Varga, M. Rotter, L. Skrbek, *Phys. Rev. B* **86**, 134515 (2012).

[69] S. Babuin, E. Varga, L. Skrbek, E. Lvêque, P.-E. Roche, *Europhys. Lett.* **106**, 24006 (2014).

[70] W. Guo, M. La Mantia, D.P. Lathrop and S.W. Van Sciver, *Proc. Natl. Acad. Sci. U.S.A.*, **111**, Supplement 1, 4653-4658 (2014).

[71] D.E. Zmeev, F. Pakpour, P.M. Walmsley, A.I. Golov, W. Guo, D.N. McKinsey, G.G. Ihas, P.V.E. McClintock, S.N. Fisher, and W.F. Vinen, *Phys. Rev. Lett.* **110**, 175303 (2013).

[72] R. Hänninen and W. Schoepe, *J. Low Temp. Phys.* **158**, 410 (2010).

[73] L. Skrbek and W.F. Vinen in *Progress in Low Temperature Physics* Vol. **XVI**, edited by W.P. Halperin and M. Tsubota (Elsevier, Amsterdam, 2008), Chapter 4.

[74] L. Gurevich, B.D. Laikhtman, *Zh. Eksp. Teor. Fiz.* **69**, 1230-1242 (1975).